Influence of Zr/Si Molar Ratio on Structure, Morphology and Corrosion Resistance of Organosilane Coatings Doped with Zirconium(IV) n-propoxide

Chun Juan Fu, Zhong Wei Zhan, Mei Yu[*], Song Mei Li, Jian Hua Liu, Lin Dong*

School of Materials Science and Engineering, Beihang University, Beijing 100191, P. R. China
[*]E-mail: yumei@buaa.edu.cn

A series of coatings with different zirconium(IV) *n*-propoxide (TPOZ) to glycidoxypropyl-trimethoxy-silane (GTMS) molar ratios (i.e. Zr/Si ratio) were prepared on AA2024-T3 aluminium substrate by dip-coating method. The particle size distribution in the mixed sols was analyzed to find possible existence forms of particles in the mixtures. The structure of coatings was investigated by using Fourier transform infrared (FTIR). The coating morphology was observed with scanning electron microscopy (SEM) and atomic force microscopy (AFM). The corrosion resistance of the coatings was evaluated by electrochemical methods, as well as neutral salt spray test. The micro-hardness of the coatings was also measured. The results indicats that the addition of TPOZ generally promotes the formation of silica network and enhances the compactness of coating matrix and oxide layer between coating and aluminium substrate. However, excessive TPOZ exceeds the ability of silica network to be loaded with, introducing incompatible ZrO_2 clusters into the coating. At Zr/Si ratio of 0.5, the doped TPOZ fully incorporates into silica network, and the coating is of the best performance.

1. INTRODUCTION

A reliable, effective and environmentally benign surface treatment is of significant importance for the performance of aluminium alloy. Given the need of replacement of traditional chromate-containing coatings, silane-derived sol-gel coatings have been gathering remarkable attention as potential alternative for aluminium alloy [1-5]. Silane coatings based on pure inorganic oxide are generally brittle and cracking sensitive. To avoid the flaws above, proper post treatments of silane coatings are needed, mostly densification. The densification of such coatings usually calls for relatively high processing temperature, for example more than 400 °C [6]. Unfortunately, high

temperatures result in metallurgical changes to aluminium alloy, which are deleterious for its intrinsic mechanical and fatigue properties [7, 8]. Consequently, novel hybrid silane coatings containing organic components [3, 9-11] and/or multi-metal alkoxides [1, 2, 12, 13] have been extensively studied in order to reduce the susceptibility to cracking and enhance the corrosion resistance. With different functional organic groups (vinyl, methacryloxy and glycidoxyproyl), the organosilane coatings exhibited better corrosion resistance [11]. The corporation of ZrO_2 and CeO_2 nano particles into TEOS/TEOCS (tetraethylorthosilicate and tetraocthylorthosilicate) system improved the electrochemical properties of the coating by a kind of self-healing mechanism [2].

The elastic organic components which usually attach to Si atom in the silane molecule are beneficial to increase the flexibility of coatings. The nano-sized oxide particles, products of hydrolysis reaction of metal alkoxides, disperse throughout the matrix to reinforce the coatings. However, excessive addition of metal alkoxide dramatically weakens the performance of coatings, even reproduces cracking [1]. It is believed that the excessive amount of metal oxide exceeds the ability of the silane coating matrix to be embedded with. Thus the coating integrity is damaged. Therefore, an essential consideration in formulating a robust sol-gel coating with multi-metal alkoxides is to maintain a proper metal alkoxide to silane ratio.

In this study, the zirconium(IV) *n*-propoxide (TPOZ) was doped into a organosilane (glycidoxypropyl-trimethoxy-silane , GTMS) solution to prepare a series of sols with various molar ratios of TPOZ/GTMS, namely Zr/Si ratio. We aimed to evaluate the influence of Zr/Si ratio on the property of mixed sols, the structure, morphology and the performance of resulted coatings on AA2024-T3 aluminium substrate.

2. MATERIALS AND METHODS

2.1. Substrate preparation

The substrate material used in the present investigation was AA 2024-T3 aluminium alloy. For most characterizations described in section 2.3 except neutral salt spray test, the alloy was cut into round samples with diameter and thickness of 20mm and 3mm, respectively. The round samples were grinded with waterproof abrasive papers of successively fine grit down to 2000 grit. After that, the samples were mechanically polished using diamond paste to a mirror polish. They were then degreased with ethanol for 10min, rinsed in distilled water and finally dried in air.

The alloy coated for neutral salt spray test was cut into sheets with dimensions 100 mm ×50 mm ×3 mm. The sheet samples were sanded to 800 grade with waterproof abrasive papers, and cleaned with the same procedure as the round samples.

2.2. Preparation of coatings

A silane solution (Si sol) was prepared by mixing glycidoxypropyl-trimethoxy-silane (GTMS, analytical, Nanjing Capatue Chemical Co., Ltd, China) with ethanol with equal volume. Distilled water

was added dropwise under stirring to enable hydrolysis of GTMS. The molar ratio of H_2O:Si was 5:1. Zirconium(IV) n-propoxide (TPOZ, 70 % w/w in n-propanol, Alfa Aesar) was independently chelated with glacial acetic acid in a volume ratio of 2:1, and stirred for 30 min in a sealed beaker. As well, distilled water with molar ratio H_2O:Zr of 4:1 was added dropwise to form Zr sol. Finally, the Zr-acetic acid complex solution was gently added into the hydrolyzed GTMS solution under stirring. The mixed sol was sealed and kept on stirring for 1 h afterward. The Zr/Si molar ratios of mixed sols were 0, 0.1, 0.2, 0.5, 1.0 and 1.5.

The coatings were fabricated on the aluminium samples by dip-coating with a withdraw speed of 1 mm/s for two times. Each immersion into the sol was of 5 min. After the first immersion, the samples were dried in air for 15 min and in oven at 60 °C for 10 min. After the second immersion, a successive curing procedure was applied: in air for 15 min, and in oven at 60 °C for 1 h, 90 °C for 30 min and 120 °C for 15 min.

2.3. Characterizations

The mixed sols with different Zr/Si ratios were analyzed by using a laser particle size analyzer (Zetasizer Nano ZS, Malvern, Britain) to determine the particle size distribution. The coatings morphology and surface roughness were investigated by using scanning electron microscopy (SEM, Apollo 300, Cam Scan, Britain) and atomic force microscopy (AFM, Veeco, USA). The Fourier transform infrared (FTIR) measurements of the coatings were performed on a Thermo Nicolet Nexus 470 Fourier transform spectrometer. The spectra were obtained at the resolution of 8 cm^{-1} and were averages of 32 scans. The range of FTIR spectra was about 600-4000 cm^{-1}.

The electrochemical tests were carried out by using an Advanced Electrochemical System (PARSTAT 2273, Princeton, USA). A three-electrode cell was employed, consisting of a saturated calomel reference electrode (SCE), a platinum foil as counter electrode and the coated samples as working electrode with a surface area of 1 cm^2. All electrochemical tests were carried out at constant temperature (30±1 °C) by putting the cell into water bath. The test solution was 0.05 M NaCl solution. The Potentiondynamic polarization tests were performed at a sweep rate of 1 mV/s. Before each measurement, the coated sample was immersed into the NaCl solution for 30 min until to get steady condition. The electrochemical impedance spectroscopy (EIS) measurements were conducted with AC excitation amplitude of 10 mV at open circuit potential. The frequency range was from 10 kHz to 10 mHz with 7 data points per decade. Before each measurement, the coated sample was immersed into the NaCl solution for 30 min until to get steady condition. Several equivalent circuits were proposed to fit the EIS data and extract related electrochemical parameters by using ZSimpWin software. In order to ensure reproducibility of the measurements, the samples were tested in triplicate.

Micro-hardness of the coatings was measured with a microhardness tester (FM-800, Future-Tech, Japan) using a 50-gF load for 15 s. The corrosion resistance of the coated samples was examined by putting them into a salt spray chamber (WYX/Q-250, YaShiLin, China).

3. RESULTS AND DISCUSSION

3.1. Particles size distribution in sols

The particle size distributions of pure Zr sol and mixed sols with different Zr/Si ratios aged for 12 h are shown in Fig. 1. The median particle sizes (D50) of pure Zr sol and Si sol (i.e. Zr/Si=0) are 5.62 and 56.44 nm, respectively. The TPOZ is chelated with glacial acetic acid to suppress hydrolysis and condensation reaction [14], in order not to form precipitations. However, a 12-h aging is enough for full hydrolysis of TPOZ to form nano-sized (D50=5.62 nm) ZrO_2 particles with narrow size distribution. The resulted Zr sol is a transparent and light yellow solution. Contrastively, the median particle size of pure Si sol is 10 times more than that of Zr sol. Generally, the acid catalysis promotes the hydrolysis reaction of alkoxysilane over condensation while base catalysis does the opposite. At pH value of 4, the hydrolysis rate reaches its maximum, yet condensation is depressed. For the pure Si sol with pH value of 5.78, the hydrolysis rate of GTMS is relatively slow [15, 16]. Since no catalysis was added, the GTMS may be partially hydrolyzed to form one or two silanols (Si-OH) per molecule as shown in Equation 1. Given the high concentration of GTMS (approx. 41 vol.%), the silanol group could condensate with alkoxy group to form Si-O-Si bond, as shown in Equation 2. Therefore, polymers with large number of silane molecules may be formed. It is worthy to mention that due to the partial hydrolysis of GTMS, a lot of residual alkoxy groups, rather than silanol groups remained in the polymers. From the viewpoint of reacting with hydroxyl compounds on the metal surface, the silanol surpasses the alkoxy. Hence, these large polymers in the pure Si sol are expected to be less reactive to form strong bonds with metal substrate.

$$H_3CO-\underset{\underset{OCH_3}{|}}{\overset{\overset{R}{\wr}}{Si}}-OCH_3 \ + \ H_2O \ \xrightarrow{\textit{hydrolysis}} \ H_3CO-\underset{\underset{OCH_3}{|}}{\overset{\overset{R}{\wr}}{Si}}-OH \ + \ CH_3OH \qquad [1]$$

$$\equiv Si-OH \ + \ H_3CO-Si\equiv \ \xrightarrow{} \ \equiv Si-O-Si\equiv \ + \ CH_3OH \qquad [2]$$
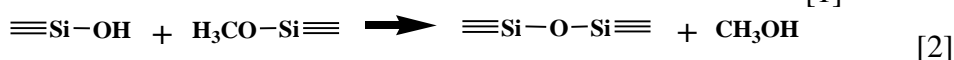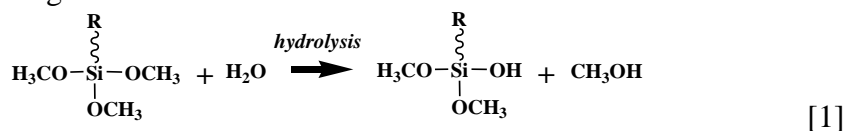
The D50 values of mixed sols are lower than that of pure Si sol, and decreased with Zr/Si ratios. The data is listed in Fig. 1. With Zr/Si ratio increasing from 0 to 0.5, only single peaks are detected in the intensity plots. Whereas, there are two peaks for Zr/Si ratios of 1.0 and 1.5, the peak positions of which are labeled in Fig. 1. It seems that different kinds of particles form in the mixed sols with high Zr/Si ratios. The changes of particle size in mixed sols are attributed to the structure evolution of oligomers formed by GTMS. The acidity nature of mixed sols with pH around 3.40-3.90 caused by glacial acetic acid in Zr sol promotes the hydrolysis of GTMS to form fully hydrolyzed silanols, and depresses the condensation of silanols to a certain extent. So the formed polymers could barely grow any larger than those in pure Si sol. Meanwhile, the hydrolyzed TPOZ [$Zr(OH)_4$] incorporates into the formation of silane polymers by condensing with silanols. These mixed polymers are composed of fully hydrolyzed products of GTMS and TPOZ. Therefore, the main difference between the polymers in mixed sols and pure Si sol was that, the polymers in mixed sols contain enough hydroxyl groups to bond with the native oxide on the metal surface.
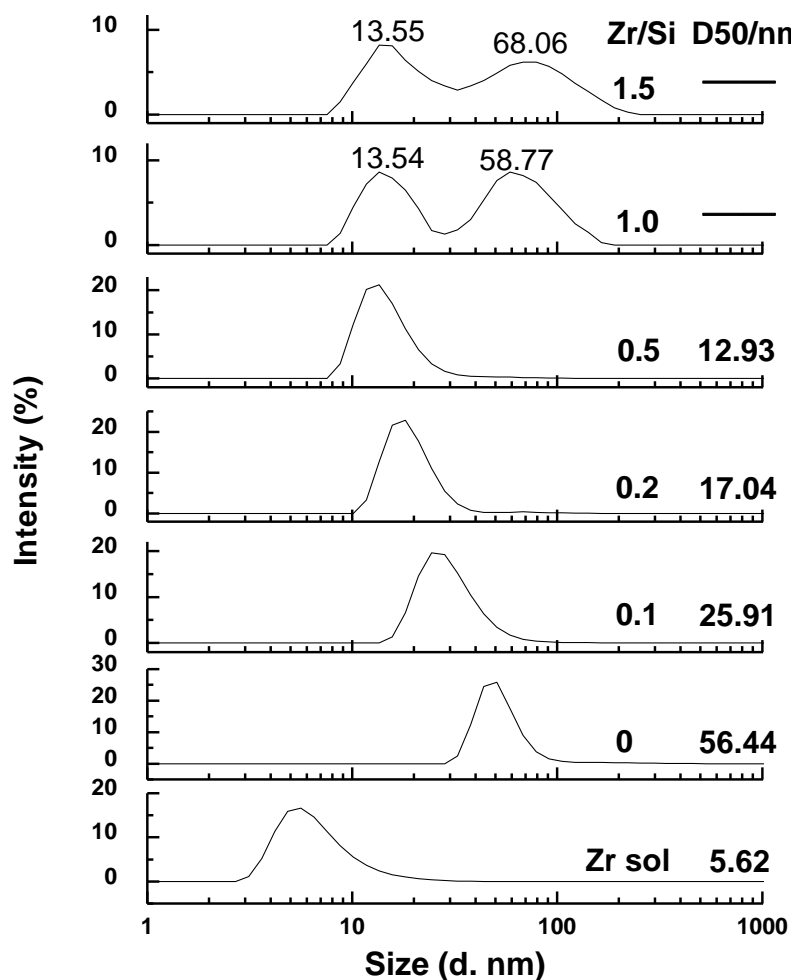
Figure 1. Particle size distributions of sols with different Zr/Si ratios aged for 12 h

However, above a Zr/Si ratio of 0.5, the silane polymers seem incapable to contain Zr species anymore. The concentrations of TPOZ in the mixed sols with Zr/Si ratio of 1.0 and 1.5 are 24.8 and 32.2 vol.%, respectively. The silane polymer is immoderately loaded with Zr species in such saturated environment for TPOZ. The particle size of the mixed polymer reaches its minimum around 13.54 nm for both sols. Considering the high reactivity of TPOZ, the excessive ZrO_2 tends to self-condense to form ZrO_2 clusters, which results in nanoscale phase segregation [17, 18]. The ZrO_2 clusters are responsible for the new peaks at 58.77 nm and 68.06 nm for Zr/Si ratio of 1.0 and 1.5, respectively. From the viewpoint of reacting with and coating the metal surface, the ZrO_2 clusters are obviously detrimental. A silane network doped with enough ZrO_2 species is beneficial to obtain dense coatings on metal surface.

3.2. Structure changes of coatings

FTIR absorbance spectra for coatings deposited on aluminium samples from sols with Zr/Si ratios ranging from 0.1 to 1.5 are shown in Fig. 2. To get a full and detailed vision, the spectra are divided into two parts with different wavenumber increments along the dash line at 1750 cm^{-1}.
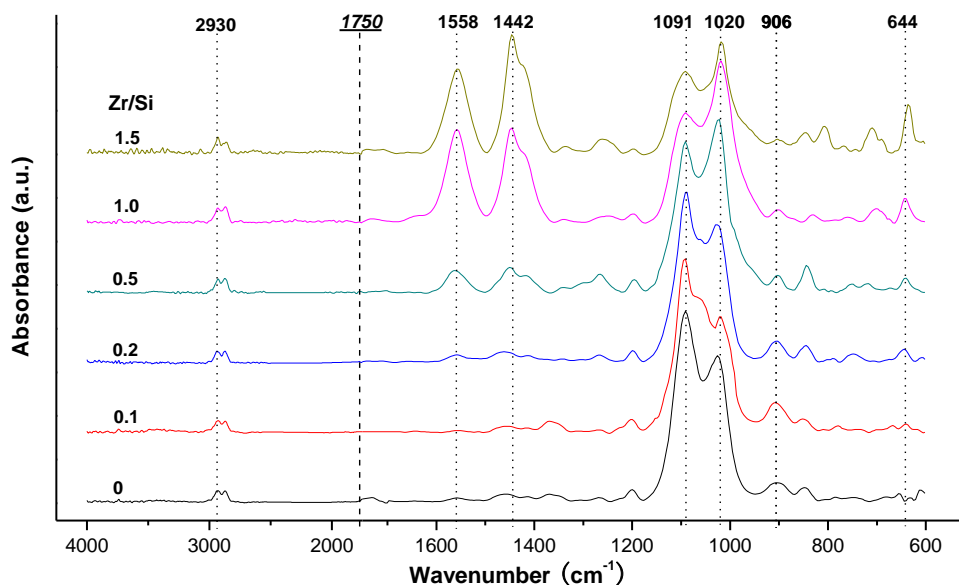
Figure 2. FTIR spectra for coatings with various Zr/Si ratios (*indicated at left*)

For all Zr/Si ratios, two noticeable peaks at 1091 and 1020 cm^{-1} are present, which are assigned to Si-O-Si stretching vibration in cage and network configurations, as shown in Fig. 3(a) and 3(b), respectively [19-23]. The absorbance in FITR spectra ranging from 1100 cm^{-1} to 1200 cm^{-1} is due to the asymmetric vibration of various cage-like structures, while absorbance in the range of 1010-1050 cm^{-1} is due to symmetric stretching in random network with lower symmetry [23, 24]. As Zr/Si ratio increases from 0 to 1.0, the ratio of absorbance at 1020 cm^{-1} to that at 1091 cm^{-1} increases. It indicates that the addition of Zr obstructs the formation of cage-like structures in the matrix of silane coating, and promotes the development of silane network. It is worthy to point out again that the cage-like structures based on partial hydrolyzed GTMS generally contain few active sites for condensation (namely -SiOH), let alone form strong covalent bonds with metallic substrates. Whereas the network structures are ended with -SiOH groups which are readily to react with silanols and metal alkoxides. The expansible network is essential to fabricate uniform and dense coatings.
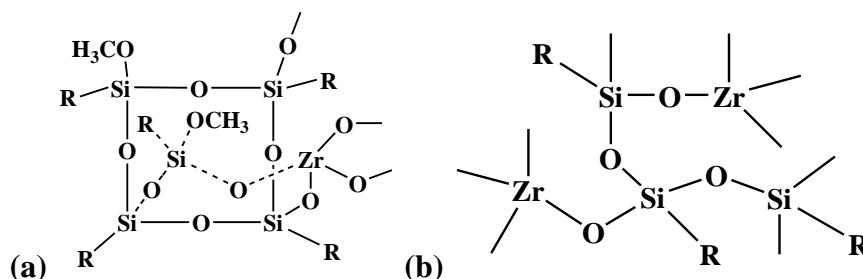
Figure 3. Structures of (a) silane cage with Zr species and (b) network with Zr species incorporated

The peak at around 906 cm^{-1} is assigned to the silanol groups [25, 26] as well as the unopened epoxy groups [21, 27]. This peak gradually decreases in intensity with Zr/Si ratio rising from 0 to 1.5,

which indicates that the amount of residual silanol groups in the coatings reduces with addition of TPOZ and epoxy groups perhaps encounter ring-opening reaction. The absorbance from 940 to 980 cm^{-1} enhances with Zr/Si ratio. It is believed absorbance in this range is attributed to Si-O-Zr bonds [26, 28]. Therefore, a hybrid network containing zirconia and organo-silica is formed in the coatings.

Two remarkable peaks appear at 1442 and 1558 cm^{-1} for coatings with Zr/Si ratios from 0.5 to 1.5, corresponding to Zr-O-C [29] and COO^--Zr bonds [30-32], respectively. However, they ae barely observed for coatings with Zr/Si ratios of 0, 0.1 and 0.2. Considering the additional peaks of particle size caused by excessive ZrO_2 clusters in the sols with Zr/Si ratio of 1.0 and 1.5, it is highly possible that these Zr-related bonds detected in FTIR are from the chelate complex between ZrO_2 clusters and acetic acid. Hence, above a Zr/Si ratio of 0.5, the silica network can hardly contain more ZrO_2, which probably exists in a form of non-chemically bonded with coating matrix. The presence of excessive ZrO_2 in the coatings also explains the change of Zr-O-Zr bond at 664 cm^{-1}. Little change is observed between Zr/Si ratios of 0.1 and 0.5, yet absorbance of Zr-O-Zr bond clearly increases with Zr/Si ratio from 1.0 to 1.5.

The peak at around 2930 cm^{-1} is from the C-H bonds in the residual carbon chains and similar for all coatings. It is worthy to note that no broad peaks are observed between 3400 and 3600 cm^{-1}, which generally belong to hydroxyl groups. This probably indicates the water and alcohol are almost fully evaporated from the coatings after the drying procedure.

3.3. Morphology and surface roughness of coatings
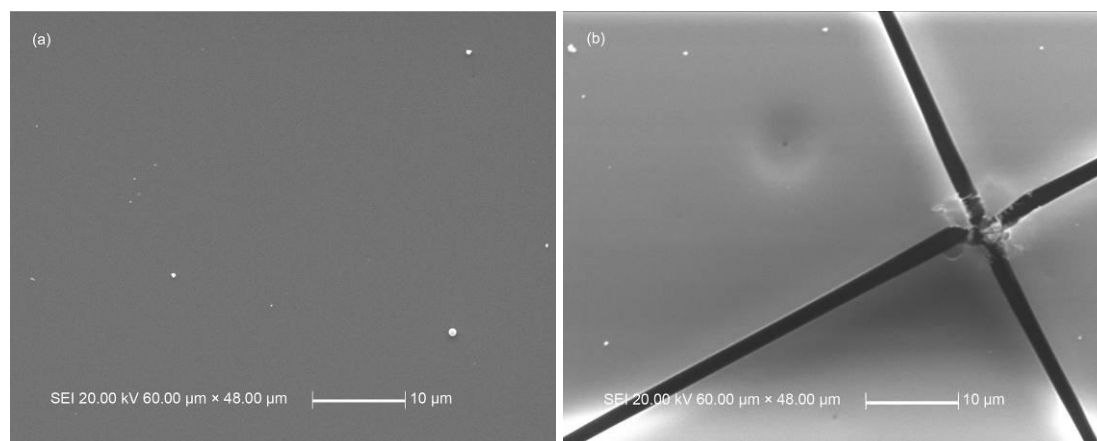
Figure 4. SEM micrographs for the surfaces of coatings with different Zr/Si ratios (a) 0.5 (×2000); (b) 1.5 (×2000)

Fig. 4 shows the SEM morphology of coating surfaces with Zr/Si ratios of 0.5 and 1.5. The coating surface with Zr/Si of 0.5 is very flat and smooth, no cracks or pinholes are observed, as shown in Fig. 4(a). Since other coatings with Zr/Si ratios of 0, 0.1, 0.2 and 1.0 share the similar morphology characteristics: flat, smooth, no cracks, they are not present here. However, there are remarkable cracks seen in Fig. 4(b) present on the surface of coating with Zr/Si of 1.5. Essentially, cracks on the surface of coating are the result of internal stress which exceeds the tolerance of the coating. In this case, high

Zr content increases the inorganic component in the coating. During the drying procedure, the ZrO_2 clusters in the coating are further dehydrated, which probably exhibit different shrinkage rate from that of the silica network. Thus, internal stress accumulates and develops, until cohesion of coating matrix (i.e. silica network) is exceeded.The cross section of coating with Zr/Si ratio of 0.5 is shown in Fig. 5. The thickness of the coating is about 2.5 µm. There is no interface detected inside the coating, which indicates the double dip-coating does not lower the adherence between the two layers. The coating is well adhered to the surface of aluminium substrate, without any cracks or pinholes. The other coatings' thicknesses are found comparable with values between 2-3 µm by using an eddy current thickness meter.
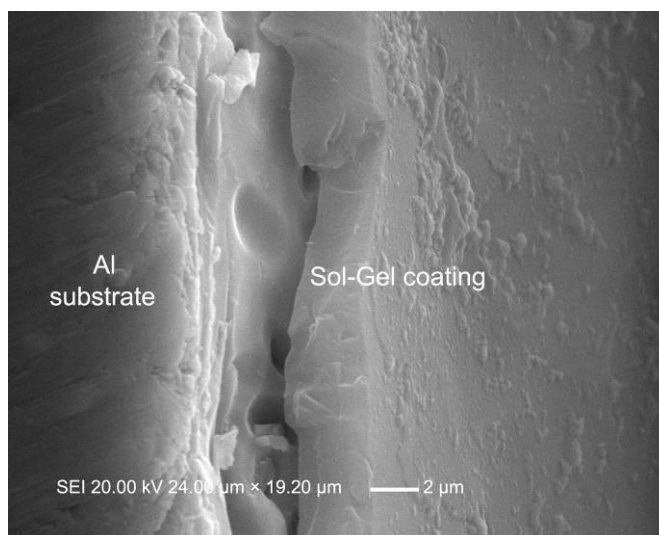
Figure 5. SEM micrograph for cross section of coating with Zr/Si ratio 0.5 (×5000)

To get a detailed influence of Zr/Si ratio on the morphology of coatings, atomic force microscopy (AFM) was applied. Fig. 6 presents the AFM morphology of coatings with different Zr/Si ratios, and the corresponding surface roughness data is listed in Table 1. In general, the surface morphology of these coatings varies significantly with Zr content. The pure Si coating (i.e. Zr/Si=0) is extremely flat and uniform, with a surface roughness Ra of 0.41 nm, as shown in Fig. 6(a). After a little amount of TPOZ added (Zr/Si=0.1), the coating surface becomes slightly uneven with Ra 0.67 nm in Fig. 6(b). As Zr/Si ratio increases to 0.2, the unevenness of the coating surface enhances, showing clearly concave-convex appearance in Fig. 6(c). The craters on the surface distributes separately. The height profile alone the white line shows a 1 nm depth of craters. The neighboring craters start to link with each other for the coating with Zr/Si of 0.5, as shown in Fig. 6(d). The sizes of craters all enlarge, with a diameter of 2-4 µm and depth of 2-3 nm for a single crater.
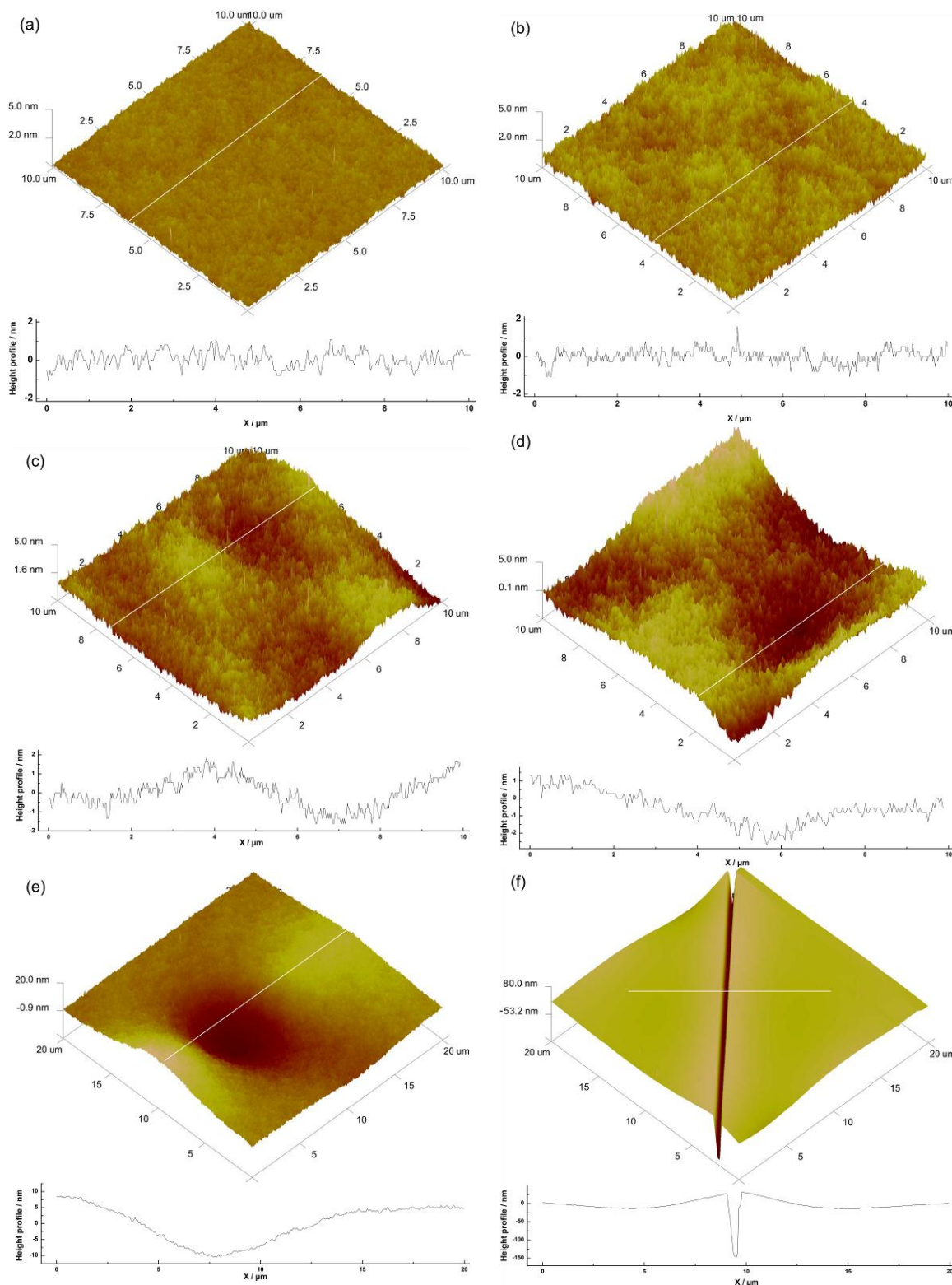
Figure 6. AFM images of coatings with different Zr/Si molar ratios (a) 0, (b) 0.1, (c) 0.2, (d) 0.5, (e) 1.0, (f) 1.5

Table 1. Surface roughness of coatings with different Zr/Si ratios

Zr/Si ratio	0	0.1	0.2	0.5	1.0	1.5
Ra /nm	0.41	0.67	1.22	2.72	5.49	—

Apparently, the morphology of coating surface is directly affected by Zr/Si ratios. The craters continuously deepen and enlarge as Zr/Si ratio reaches to 1.0. The height profile of this coating reveals the crater is about 6-8 μm in size and 10 nm in depth. In order to get a full vision of the crater, the AFM image of this coating covers an area of 20 μm×20 μm, larger than those of previous coatings. The craters may be related to the repolymerization reactions in the coating matrix. During the drying process, the heat promotes the residual uncondensed silanols to form Si-O-Si bonds, resulting in local shrinkage. Meanwhile, the excessive ZrO_2 clusters can also condense with the silica network to form Zr-O-Si bonds, and gradually dissolves into neighboring coating matrix. The products of these reactions, mainly water, easily evaporate away from the coating. The reactions bring in local internal stress as well. Therefore, concave-convex morphology with craters appears.

The AFM morphology of coating with Zr/Si of 1.5 is well agreed with that observed by SEM. Clear cracks spreads across the surface with depths more than 100 nm. The roughness data is meaningless for this coating.

3.4. Electrochemical impedance of coatings

The electrochemical impedance spectra are useful to provide modeling method of the physicochemical processes of the coated samples during immersion tests. By applying suitable equivalent circuit, responses of different components of the coatings can be separately presented, such as capacitance and resistance of the protective layers, and the oxide layer. The evolution of these parameters reveals structural changes of the coatings during immersion. Fig. 7 shows the evolution of impedance spectra of coatings with different Zr/Si ratios for various immersion times.

The impedance spectra of pure Si coating (Zr/Si=0.0) are shown in Fig. 7(a). Two time constants are observed after 2h of immersion. One is responsible for the relaxation process of the coating at high frequency ($10^{4.5}$ Hz), and another in middle-low frequency range ($10^{3.5}$-10^{-2} Hz) is resulted from the inorganic oxide layer between the metal surface and pure Si coating. A 2-day immersion does not change the resistance and phase angle curves remarkably. However, the resistance of the coating shows a significant decrease after 10 days of immersion. The phase angle of the time constant at high frequency decreases for about 10 degrees, while the phase of time constant in low frequency range remains. It makes sense because after a 10-day immersion, electrolyte and water probably penetrate through the coating and begin to attack the oxide layer. A sharp drop of phase angle appears after 20 days of immersion, with continuous decline of total impedance value at 10^{-2} Hz. The time constant at high frequency vanishes, indicating the coating entirely loses resistance to electrolyte and water. A subtle plateau of impedance at low frequency suggests the corrosion of aluminium substrate is potentially in progress.
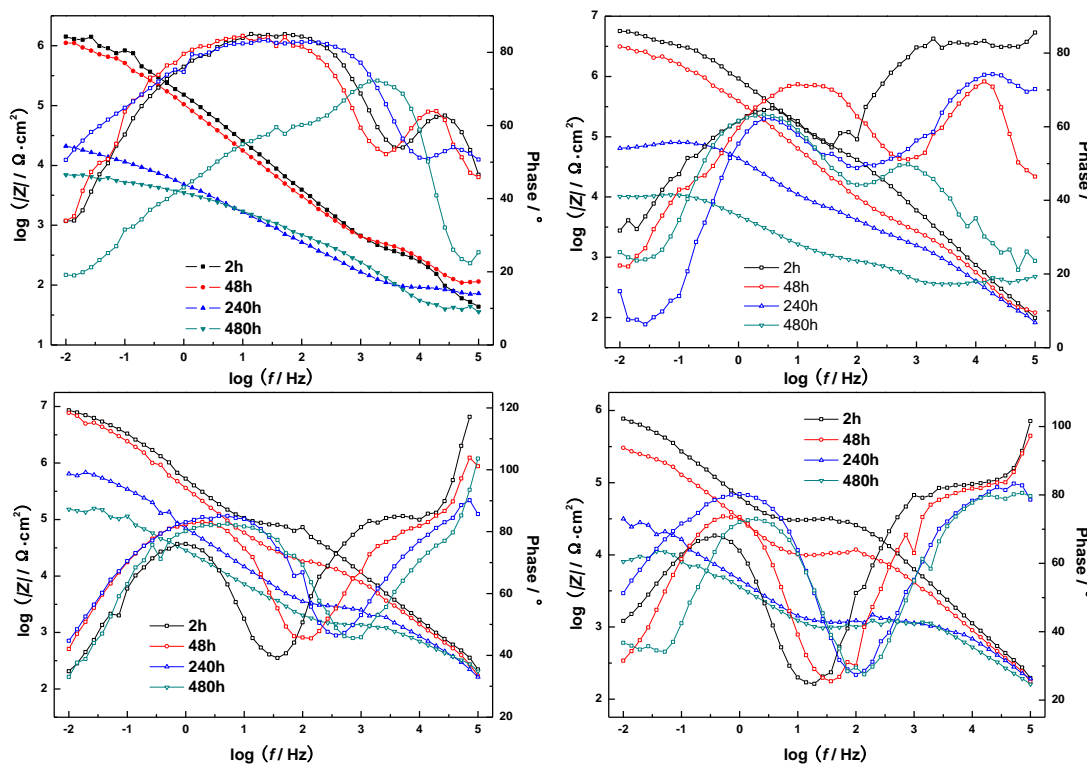
Figure 7. Evolution of EIS plots of coatings with different Zr/Si ratios during immersion in 0.05 M NaCl solution: (a) 0.0; (b) 0.2; (c) 0.5; (d) 1.0

Fig. 7(b) presents the EIS plots of coating with Zr/Si ratio of 0.2. The incorporation of TPOZ positively affects the corrosion protection of the coating. The total impedances at 10^{-2} Hz of this coating are all higher than those of pure Si coating at same immersion times. After 10 days of immersion, a third time constant appears in range of $10^{-1.5}$-10^{-2} Hz, suggesting the corrosion of aluminium substrate occurs.

The EIS curves of coating with Zr/Si ratio of 0.5 are shown in Fig. 7(c). With higher TPOZ content, the initial impedance value at low frequency (10^{-2} Hz) reaches 10^7 $\Omega \cdot cm^2$, the highest value for all tested coatings. Moreover, the impedance plot barely changes after 2 days of immersion. The low frequency impedance value remains $10^5 \Omega \cdot cm^2$ even after 20 days of immersion. Impressively, no additional time constant appears at low frequencies, demonstrating the oxide layer and the coating are much more durable than others. The incorporation of TPOZ with Zr/Si ratio of 0.5 leads to the coating with significant better barrier properties and higher stability against electrolytic attack.

Fig. 7(d) shows the evolution of impedance spectra of coating with Zr/Si ratio of 1.0. Similar with pure Si coating and coating with Zr/Si=0.2, this coating also fails to avoid the third time constant at low frequencies, which is related with corrosion of aluminium substrate. Detected here is a drop of more than two orders of magnitude of low frequency impedance value. The large craters observed in AFM are responsible for the coating degradation. With less dense structure than the coating matrix, these craters are much more easily disintegrated in the long-time immersion.

By fitting the experimental EIS data with proper equivalent circuits, quantitative values of different components of coatings can be derived. In this case, two equivalent circuits are proposed to

fit the experimental data of the coatings at different times, as shown in Fig. 8. The equivalent circuit in Fig. 8(a) is for the coatings without signs of corrosion of aluminium substrate, and for the coatings with a third time constant at low frequencies, circuit in Fig. 8(b) is used. In the circuits, R_{sol} is the resistance of solution, Q_{coat} and R_{coat} are the capacitance and resistance of the sol-gel coating, while Q_{ox} and R_{ox} are those of the inorganic oxide layer between the metal surface and the coating. After corrosion of aluminium substrate occurred, another panel of elements, Q_{dl} and R_{ct}, is added, representing the capacitance of double layer and resistance of charge transfer process, respectively.
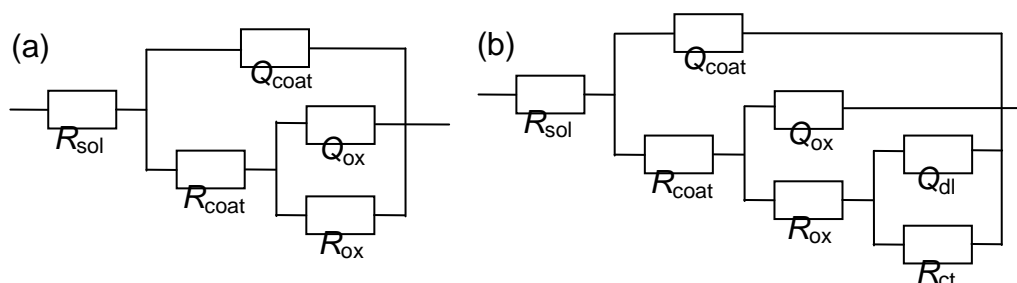
Figure 8. Equivalent circuits for different stages during immersion: (a) Without and (b) with corrosion of Al substrate

Table 2 lists the derived parameters of four coatings during continuous immersion, and evolution of these parameters is shown in Fig. 9. All the four coatings show the highest coating resistance, R_{coat}, at the beginning of immersion followed by drop, as shown in Fig. 9(a). After 240h of immersion, changes of coating resistances R_{coat} are inconsequential. For all coatings, the one with Zr/Si ratio of 0.5 exhibited the highest coating resistance during most time of immersion. The capacitances of coatings, Q_{coat}, generally increase with immersion time in Fig. 9 (b). The capacitance of coating with Zr/Si ratio of 0.5 keeps relatively stable after 48h of immersion. The drop of coating resistance as well as the increase of capacitance of coating is essentially disadvantageous for the protection performance of coatings. Bearing high coating resistance and low capacitance, the Zr/Si 0.5 coating exceeds others in coating properties and stability. Considering the moderately roughened morphology and network-rich structure, the good performance of Zr/Si 0.5 coating is probably resulted from its proper component ratio. It is reasonable to reckon that at ratio of 0.5, the doped TPOZ is fully embedded into the silica network in form of reactive segment as shown in Fig. 3(b) rather than ZrO_2 clusters, acting as enhancing phase in the coating matrix. Therefore, the corrosion resistance and stability of the coating are improved.

According to some researchers [33, 34], the oxide layer between sol-gel coating and metal surface is basically composed of metal-O-Si covalent bonds, in this case Al-O-Si and Al-O-Zr bonds. This oxide layer is the last barrier to prevent substrates from being attacked by corrosive agents and water. Fig. 9(c) and (d) are the changes of resistance R_{ox} and capacitance Q_{ox} of the oxide layer with immersion time. Undoubtedly, all resistances of oxide layers, R_{ox}, decrease with time. Among them, R_{ox} of pure Si coating loses nearly three orders of magnitude after 480 h of immersion, whereas that of Zr/Si 0.5 coating loses only one, preserving 1.587E5 $\Omega \cdot cm^2$ at the end of immersion.

Table 2. Parameters of four coatings obtained from fitting results with different equivalent circuits

Coatings	Immersion time h	R_{coat} $\Omega \cdot cm^2$	Q_{coat} $F \cdot cm^{-2}$	R_{ox} $\Omega \cdot cm^2$	Q_{ox} $F \cdot cm^{-2}$
Zr/Si=0.0	2	1174	4.372E-8	4.954E6	1.465E-7
	48	573.7	1.325E-7	8.227E5	8.787E-8
	240	166.5	1.643E-7	1.773E5	9.772E-8
	480	175.3	1.968E-7	4008	1.452E-6
Zr/Si=0.2	2	5.850E4	5.067E-8	4.948E6	1.864E-7
	48	3405	9.089E-8	4.138E6	3.549E-7
	240	4350	2.414E-7	7.225E4	6.682E-7
	480	2247	1.543E-7	1.298E4	1.965E-6
Zr/Si=0.5	2	1.177E5	2.599E-9	8.341E6	1.21E-8
	48	7.352E4	2.376E-8	7.855E6	6.953E-8
	240	7089	2.598E-8	6.167E5	5.805E-8
	480	4277	3.687E-8	1.587E5	8.748E-8
Zr/Si=1.0	2	7.435E4	2.088E-8	6.332E5	4.121E-7
	48	6.205E4	2.703E-8	5.238E5	4.026E-7
	240	6028	1.558E-8	3.000E4	7.637E-8
	480	5997	3.749E-8	1.418E5	4.556E-7
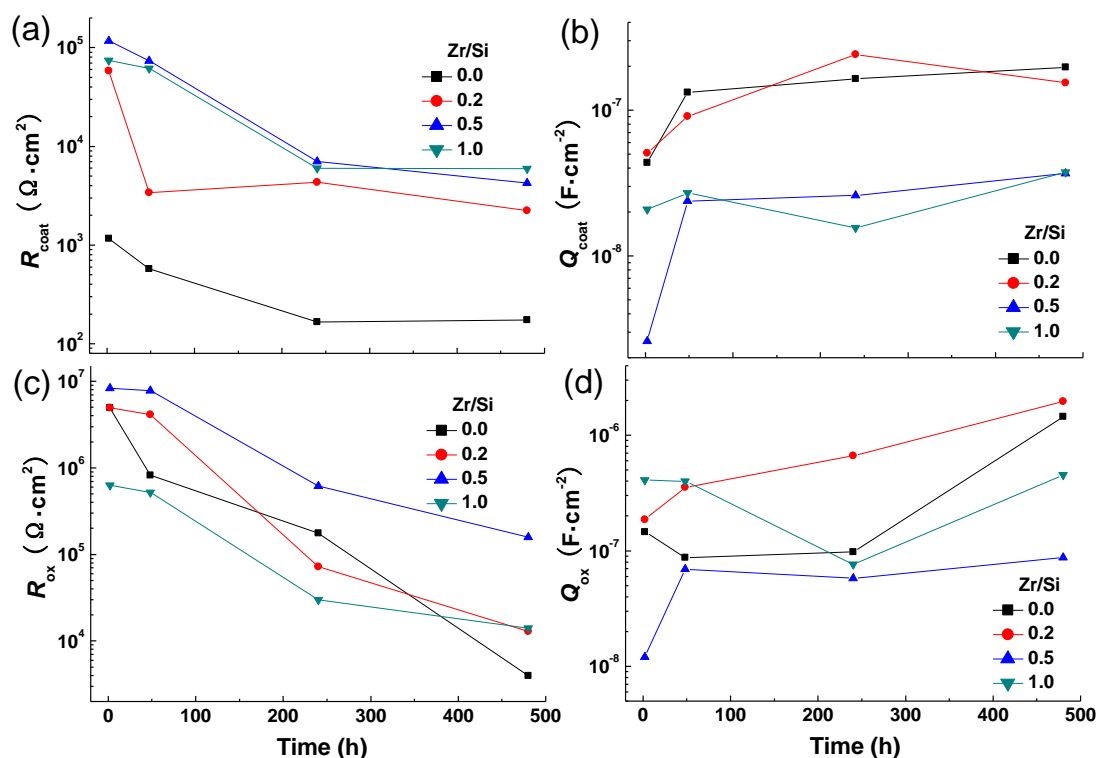
Figure 9. Evolution of parameters (a) R_{coat}, (b) Q_{coat}, (c) R_{ox} and (d) Q_{ox} of four coatings during immersion in 3.5 wt.% NaCl solution

The drop of R_{ox} is due to the water uptake, yet the extent of the drop indicates the stability of oxide layer. Interestingly, the capacitance of oxide layer, Q_{ox}, of Zr/Si 0.5 coating shows remarkable stability even after 480 h of immersion. However, the Q_{ox} of other coatings changes a lot after the immersion. As shown in Fig. 2 and 3, the addition of TPOZ promoted the formation of silica network. Thus more active sites (i.e. Si/Zr-O-) are available to bond with aluminium surface, which directly increases the Al-O-Si/Zr bond density across the substrate/coating interface and enhances the compactness of resulted oxide layer. However, ZrO_2 clusters generated by excessive TPOZ, for instance coatings with Zr/Si ratio of 1.0 and 1.5, are dispersed in the coating and harm the integrity of oxide layer. Conclusively, the coating with Zr/Si ratio of 0.5 exhibits the best compactness among all tested coatings.

3.5. Micro-hardness of coatings

Concededly, the addition of TPOZ improves the compactness of both the coating matrix and the oxide layer [35-36]. The sol–gel films containing zirconia nanoparticles present improved barrier properties[36]. As a result, the practical performance of the coated aluminium samples is leveled up, for example micro-hardness and neutral salt spray durability. Fig. 10 presents the micro-hardness of coatings with various Zr/Si ratios. Clearly, the coating with Zr/Si ratio of 0.5 reaches the highest hardness. This further confirms the conclusion expounded above that at Zr/Si ratio of 0.5, the doped TPOZ acts as enhancing phase in the coating matrix without introduction of incompatible ZrO_2 clusters, resulting in a compact and robust coating.
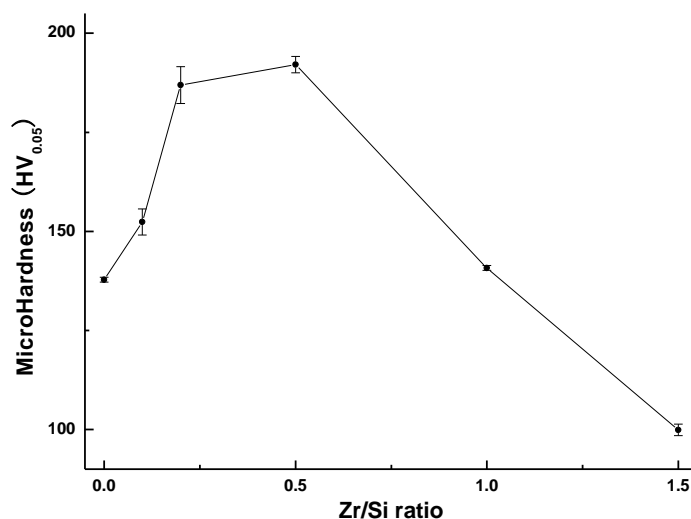
Figure 10. Influence of Zr/Si ratio on the micro-hardness of coated Al substrates

3.6. Corrosion resistance of coatings

The potentiodynamic responses of coatings with different Zr/Si ratios are shown in Fig. 11. The pure Si coating exhibits the most negative corrosion potential E_{corr} with a value of -0.72 V. The

presence of TPOZ in the coatings shifts the corrosion potential in the anodic direction. The E_{corr} of Zr/Si=0.5 coating reaches -0.50 V as the most positive. The corrosion current densities of the anodic branch generally become smaller with increasing Zr/Si ratios from 0.1 to 0.5. This perhaps is resulted by the enhancement of coating matrix by incorporation of TPOZ as discussed in previous sections. The corrosion current density of Zr/Si 1.0 coating dramatically increases, which is probably caused by the enlarged craters as ready access paths for electrolyte to reach the alloy-film interface. The coating with Zr/Si ratio of 1.5 barely protects the metal substrate beneath, with a sharp increase in corrosion current density once the positive potential is applied. This is no doubt ascribed by the cracks observed in the SEM and AFM images.
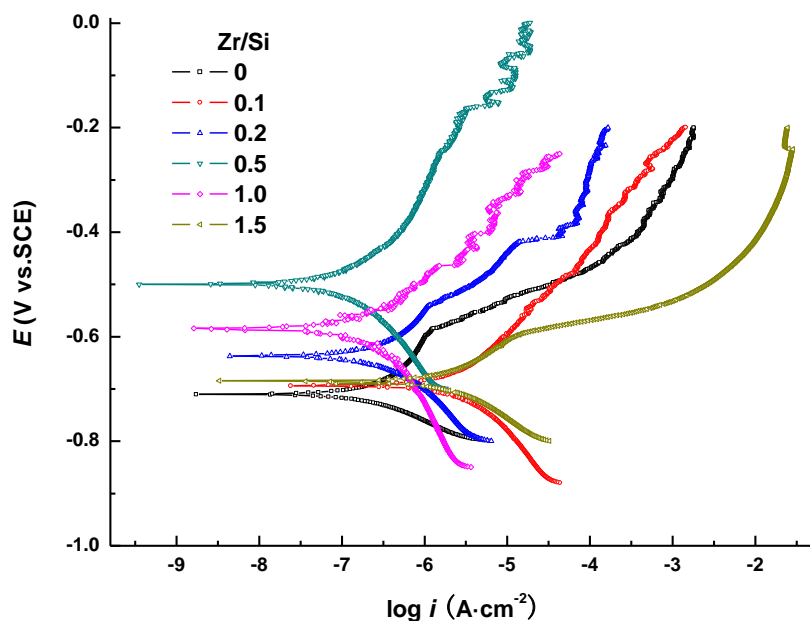
Figure 11. Potentiodynamic polarization curves of coatings with different Zr/Si ratios
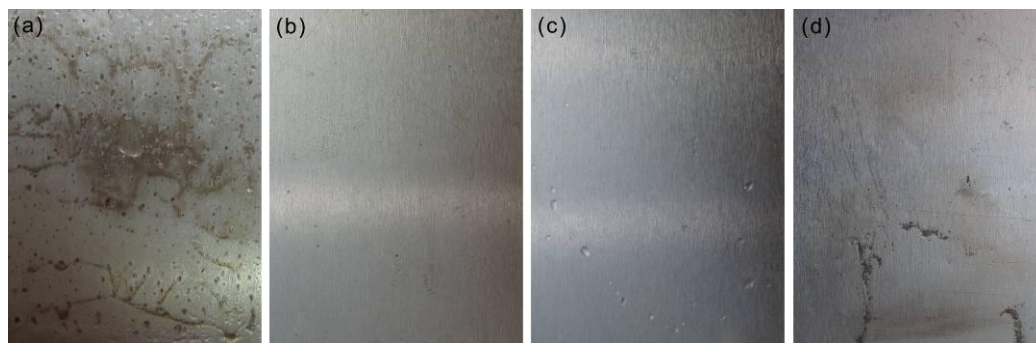
Figure 12. Optical images of coatings after 168 h in a salt spray chamber with different Zr/Si ratios: (a) 0; (b) 0.1; (c) 0.5; (d) 1.0

The neutral salt spray test is applied to evaluate the corrosion resistance of the coated aluminium substrates in severe environment. Fig. 12 shows the optical images of four coatings after a

168-h exposure in 5 wt.% NaCl neutral salt spray chamber. The pure Si coating in Fig. 12(a) is badly damaged, with a large number of pitting sites across the surface. Pitting corrosion is also observed for coatings with Zr/Si ratios of 0.1 and 1.0 in Fig. 12(b) and (d). As expected, no pitting is detected on the surface of Zr/Si 0.5 coating in Fig. 12(c). The corrosion resistance of these coatings in salt spray test generally agrees with results of electrochemical measurements.

4. CONCLUSION

The influence of Zr/Si molar ratio on the structure, morphology and corrosion resistance of organosilane coatings was investigated. The addition of TPOZ promotes the formation of silica network and incorporates into the coating matrix as reactive segments. The modified network provides more active hydroxyl groups to covalently bond with the metal surface. However, excessive TPOZ exceeds the ability of silica network to be loaded with. The surplus TPOZ forms ZrO_2 clusters, which is incompatible with coating matrix and harms the integrity of coating by introducing remarkable internal stress, even cracks. At Zr/Si ratio of 0.5, the doped TPOZ fully incorporates into the coating without ZrO_2 clusters. Bearing high content of silica network, this coating exhibits compact morphology, high micro-hardness and excellent corrosion resistance.

References

1. Z. Feng, Y. Liu, G.E. Thompson, P. Skeldon. *Electrochim. Acta*, 55 (2010) 3518.
2. E. Gonzalez, J. Pavez, I. Azocar, J.H. Zagal, X. Zhou, F. Melo, G.E. Thompson and M.A. Páez. *Electrochim. Acta*, 56 (2011) 7586.
3. A.-P. Romano, M. Fedel, F. Deflorian and M.-G. Olivier. *Prog. Org. Coat.,* 72 (2011) 695.
4. D. Wang, G.P. Bierwagen. *Prog. Org. Coat.,* 64 (2009) 327.
5. M.L. Zheludkevich, I.M. Salvado, M.G.S. Ferreira. *J. Mater. Chem.,* 15 (2005) 5099.
6. S. Sakka. *Kluwer Academic Publishers*, 2004.
7. K. Kato. *J. Mater. Sci.,* 27 (1992) 1445.
8. K. Kato. *J. Mater. Sci.,* 28 (1993) 4033.
9. A. Yabuki, H. Yamagami, K. Noishiki. *Mater. Corros.,* 58 (2007) 497.
10. C.F. Malfatti, T.L. Menezes, C. Radtke, J. Esteban, F. Ansart, J.P. Bonino. *Mater. Corros.,* Article in Press (2011).
11. Y. Liu, D. Sun, H. You, J.S. Chung. *Appl. Surf. Sci.,* 246 (2005) 82.
12. N.P. Tavandashti, S. Sanjabi, T. Shahrabi. *Mater. Corros.,* 62 (2011) 411.
13. M.L. Zheludkevich, R. Serra, M.F. Montemor, I.M.M. Salvado, M.G.S. Ferreira. *Surface & Coatings Technology,* 200 (2006) 3084.
14. S. Baroux-Doeuff, C. Sancez, Mater. *Res. Bull.,* 29 (1994) 1.
15. A.V. Cunliffe, S.Evans, D.A.Tod, S.A. Torry, P. Wylie. *Int. J. Adhes. Adhes.,* 21 (2001) 287.
16. S.A. Torry, A. Campbell, A.V. Cunliffe, D.A. Tod. *Int. J. Adhes. Adhes.,* 26 (2006) 40.

17. B. Julián, C. Gervais, E. Cordoncillo, P. Escribano, F. Babonneau, C. Sanchez. *Chem. Mater.,* 15 (2003) 3026.
18. B. Julián, C. Gervais, M.-N. Rager, J. Maquet, E. Cordoncillo, P. Escribano, F. Babonneau, C. Sanchez. *Chem. Mater.,* 16 (2004) 521.
19. F. Iacopi, Y. Travaly, B. Eyckens, C. Waldfried, T. Abell. *J. Appl. Phys.,* 99 (2006) 503.
20. W.-C. Liu, C.-C. Yang, W.-C. Chen, B.-T. Dai, M.-S. Tsai. *J. Non-Cryst. Solids,* 311 (2002) 233.
21. J. Mu, Y. Liu, S. Zheng. *Polymer,* 48 (2007) 1176.
22. M.S. Oliver, K.Y. Blohowiak, R.H. Dauskardt. *J. Sol-Gel Sci. Technol.*, 55 (2010) 360.
23. E.S. Park, H.W. Ro, C.V. Nguyen, R.L. Jaffe, D.Y. Yoon. *Chem. Mater.,* 20 (2008) 1548.
24. J.F.J. Brown, J. Am. *Chem. Soc.,* 87 (1965) 4317.
25. W.E. Wallace, C.M. Guttman, J.M. Antonucci. *Polymer,* 41 (2000) 2219.
26. L. Armelao, S. Gross, K. Müller, G. Pace, E. Tondello, O. Tsetsgee, A. Zattin. *Chem. Mater.,* 18 (2006) 6019.
27. B. Alonso, D. Massiot, F. Babonneau, G. Brusatin, G.D. Giustina, T. Kidchob, P. Innocenzi. *Chem. Mater.,* 17 (2005) 3172.
28. J.-Y. Bae, S. Yang, J.H. Jin, K. Jung, J.-S. Kim, B.-S. Bae. *J. Sol-Gel Sci. Technol.,* 58 (2011) 114.
29. S.K. Tiwari, J. Adhikary, T.B. Singh, R. Singh. *Thin Solid Films,* 517 (2009) 4502.
30. C. Barglik-Chory, U. Schubert. *J. Sol-Gel Sci. Technol.,* 5 (1995) 135.
31. E. Minor-Pérez, R. Mendoza-Serna, J. Méndez-Vivar, R.C. Pless, D. Quintana-Zavala, R. Torres-Robles. *J. Porous Mater.,* 13 (2006) 13.
32. J. Méndez-Vivar, R. Mendoza-Serna, L. Valdez-Castro. *J. Non-Cryst. Solids,* 288 (2001) 200.
33. J.S. Quinton, P.C. Dastoor. *J. Mater. Sci. Lett.,* 18 (1999) 1833.
34. J. Kim, P.C. Wong, K.C. Wong, R.N.S. Sodhi, K.A.R. Mitchell. *Applied Surface Science,* 253 (2007) 3133.
35. M. L. Zheludkevich, R. Serra, M. F. Montemor, Ma´rio G.S. Ferreira. *Electrochem Communic*, 7 (2005) 836.
36. M.L. Zheludkevich, R. Serra, M.F. Montemorb, K.A. Yasakau, I.M. Miranda Salvado, M.G.S. Ferreira. *Electrochim. Acta*, 51 (2005) 208.